

# Energy & Environmental Science

Accepted Manuscript



This is an *Accepted Manuscript*, which has been through the Royal Society of Chemistry peer review process and has been accepted for publication.

*Accepted Manuscripts* are published online shortly after acceptance, before technical editing, formatting and proof reading. Using this free service, authors can make their results available to the community, in citable form, before we publish the edited article. We will replace this *Accepted Manuscript* with the edited and formatted *Advance Article* as soon as it is available.

You can find more information about *Accepted Manuscripts* in the [Information for Authors](#).

Please note that technical editing may introduce minor changes to the text and/or graphics, which may alter content. The journal's standard [Terms & Conditions](#) and the [Ethical guidelines](#) still apply. In no event shall the Royal Society of Chemistry be held responsible for any errors or omissions in this *Accepted Manuscript* or any consequences arising from the use of any information it contains.

# A generalised space-charge theory for extended defects in oxygen-ion conducting electrolytes: from dilute to concentrated solid solutions $\ddagger$

David S. Mebane<sup>\*a</sup> and Roger A. De Souza<sup>b</sup>

Received Xth XXXXXXXXXXXX 20XX, Accepted Xth XXXXXXXXXXXX 20XX

First published on the web Xth XXXXXXXXXXXX 200X

DOI: 10.1039/b000000x

**Broader context:** A long-term aim of the solid state ionics community is to optimise the total conductivity of polycrystalline oxides based on ceria or zirconia for application as the oxygen-ion conducting electrolyte in intermediate-temperature solid oxide fuel cells (IT-SOFC). As the total conductivity of such materials includes contributions both from a conductive bulk phase and from less conductive grain boundaries, optimisation requires a deep, quantitative understanding of point-defect behaviour both in the bulk and at grain boundaries. In particular, interactions between point defects need to be taken into account, since defect concentrations in such materials are well beyond the dilute limit. We propose a theoretical framework that is able to predict point-defect behaviour at grain boundaries in concentrated solid solutions.

**Abstract:** The standard Poisson–Boltzmann approach to modeling the near-interface defect behaviour in solid electrolytes performs well at low dopant concentrations but its applicability is questionable at higher dopant levels where interactions become important. Here we present a new approach, which combines Poisson–Boltzmann with the Cahn–Hilliard model for concentrated solid solutions. This ‘Poisson–Cahn’ theory yields activity coefficients for point defects that consider both local and non-local chemical interactions. Taking the fluorite-structured solid solution  $\text{CeO}_2\text{–Gd}_2\text{O}_3$  as a model system, we predict defect behaviour near grain boundaries over the entire concentration range. Examination of the near-interface defect-concentration and electrostatic-potential profiles reveals behaviour that matches existing space-charge theory at low overall dopant concentrations, becoming more complex, in accord with experiment and atomistic simulations, as concentrations increase. Inclusion of an existing conductivity model that considers the effects of local dopant concentration leads to the successful prediction of both bulk and total (bulk + grain boundary) conductivities in both concentrated and dilute cases. The Poisson–Cahn approach is not limited to grain boundaries in oxygen-ion conducting fluorite oxides, but is applicable to all extended defects—grain boundaries, surfaces and dislocations—in ion-conducting systems.

Solid electrolytes based on zirconia,  $\text{ZrO}_2\text{–M}_2\text{O}_3$ , or ceria,  $\text{CeO}_2\text{–M}_2\text{O}_3$ , are the best known, the most thoroughly studied and the most widely used oxygen-ion conducting electrolytes.<sup>1–4</sup> The ionic conductivity of such crystalline solids at elevated temperatures easily exceeds  $10^{-1}$  S cm<sup>-1</sup>, a value comparable to the ionic conductivity of aqueous solutions at room temperature. And, as high as these values are, even higher values would be attainable were it not for two frustrating issues.

The first concerns the bulk conductivity. The  $\text{ZrO}_2$  or  $\text{CeO}_2$  lattice is partially substituted with  $\text{M}_2\text{O}_3$  in order to generate ionic charge carriers, namely, oxygen vacancies. The

ionic conductivity  $\sigma$  does not, however, increase monotonically with increasing charge-carrier concentration, *i.e.*, with increasing vacancy site fraction  $n_v$ , to peak at  $n_v = 0.5$  [for non-interacting particles,  $\sigma \propto n_v(1 - n_v)$ ]; instead the ionic conductivity peaks much earlier, at around  $n_v \approx 0.04$ . This behaviour can be explained quantitatively in terms of defect interactions:<sup>5–11</sup> attractive interactions between acceptor  $M^{3+}$  cations and oxygen vacancies; repulsive interactions between the oxygen vacancies themselves; and increased activation enthalpies of migration for oxygen vacancies adjacent to  $M^{3+}$  cations.

The second issue is that the conductivity of polycrystalline samples is only a small fraction of the conductivity of the corresponding single-crystal samples. In other words, grain boundaries (GBs) are regions of strongly decreased conductivity. Early investigations found highly resistive second phases based on  $\text{SiO}_2$  separating individual grains.<sup>12–18</sup> Low GB conductivity persisted, however, in ceramics with clean GBs—that is, on removal of these second phases.<sup>19–24</sup> This intrinsic

¶ Dedicated to Prof. Joachim Maier on the occasion of his 60<sup>th</sup> birthday.

‡ Electronic Supplementary Information (ESI) available: MATLAB m-files. See DOI: 10.1039/b000000x/

<sup>\*a</sup> Department of Mechanical and Aerospace Engineering, West Virginia University, USA. Phone: +1-304-293-3426; Fax: +1-304-293-6689; E-mail: David.Mebane@mail.wvu.edu

<sup>b</sup> Institute of Physical Chemistry, RWTH Aachen University, 52056 Aachen, Germany. E-mail: desouza@pc.rwth-aachen.de

sic GB resistance is attributed to a space-charge effect: the re-distribution of oxygen vacancies from the bulk to the GB core<sup>23,25,26</sup> generates positively charged GBs and negatively charged space-charge zones, in which oxygen vacancies are strongly depleted and acceptor-dopant cations, if sufficiently mobile, are accumulated. It is the strong depletion of oxygen vacancies in the space-charge zones immediately adjacent to the GB that is responsible for the diminished GB conductivity.

The current model of space-charge zones that is applied quantitatively to GBs in  $ZrO_2-M_2O_3$  and  $CeO_2-M_2O_3$  is based on two assumptions. First, that the electrochemical potential of the mobile defect ‘def’ takes the standard form,<sup>27–29</sup>

$$\tilde{\mu}_{\text{def}} = \mu_{\text{def}}^{\circ} + RT \ln n_{\text{def}} + z_{\text{def}} F \phi, \quad (1)$$

where  $\mu_{\text{def}}^{\circ}$  is the standard chemical potential of def; and  $n_{\text{def}}$  and  $z_{\text{def}}$  are the site fraction and charge number of def, respectively. In essence, point defects are treated in the simplest terms of dilute, non-interacting moieties. Eqn (1) and the requirement that electrochemical potentials are constant throughout the bulk lead to the Boltzmann model for the local ion density. The second assumption is that material parameters, such as standard defect chemical potentials, defect mobilities, *etc.*, exhibit step functions as the system is traversed from bulk, through the GB core, to the bulk.<sup>30</sup> That is, space-charge layers are assumed to be regions of constant defect mobilities, but of altered defect concentrations. It is the difference in the standard chemical potential of oxygen vacancies in GB and bulk that drives the formation of space-charge layers.<sup>23,25,26,29</sup>

While both assumptions are reasonable at low  $M_2O_3$  levels, validity is lost when treatments of bulk defect chemistry require defect–defect interactions to be taken into account, as is generally the case for dopant concentrations of 1% or higher.<sup>5–11</sup> Indeed, there are already some indications of more complicated behaviour at high dopant levels in the literature.<sup>23,26,31–33</sup> Tschöpe *et al.* experimentally determined the bulk and total conductivities (the latter includes GB contributions) of a range of  $CeO_2-Gd_2O_3$  compositions; dilute space-charge theory, however, only predicted the GB conductivity of the weakly doped compositions.<sup>23</sup> Kim *et al.*<sup>31</sup> found, for a concentrated  $CeO_2-Y_2O_3$  ceramic, discrepancies between GB space-charge potentials obtained by two different analytical approaches, one of which relies on dilute space-charge theory. Shibata *et al.*<sup>32</sup> examined a special boundary in  $(Zr,Y)O_2$  with Transmission Electron Microscopy (TEM) and measured Y segregation profiles that extended several nm, an order of magnitude larger than the expected Debye length. And Lee *et al.* performed atomistic simulations of concentrated  $(Ce,Gd)O_2$  and observed co-accumulation of dopants and oxygen vacancies close to grain boundaries<sup>26</sup> and surfaces<sup>33</sup> followed by short regions of vacancy depletion—behaviour that is inconsistent with dilute space-charge theory.

In this study we present a framework that is able to model

defect re-distribution at grain boundaries over the entire concentration range, from dilute (doped) systems, all the way up to concentrated solid solutions. We focus on  $CeO_2$  because the material is cubic over the entire concentration range (in contrast to  $ZrO_2$ ). For simplicity we consider only two defects (acceptor dopants and charge compensating oxygen vacancies) and we assume both to be mobile at all temperatures. Additional charge carriers (*e.g.* electrons) or a more realistic treatment of cation mobility (finite at sintering temperatures, but zero at lower (measurement) temperatures<sup>23</sup>) are easy to include but here would divert attention away from this first presentation of the framework.

The framework replaces the Boltzmann model for the local ion density with the Cahn–Hilliard theory of inhomogeneous systems.<sup>34,35</sup> For an ionic solid with mobile acceptor dopants (site fraction  $n_a$ ) and mobile, charge-compensating oxygen vacancies (site fraction  $n_v$ ), electrochemical potentials can be derived by taking appropriate variational derivatives of a free energy functional that includes terms for defect interactions and gradient effects (for mathematical details see Refs. [34–36] and [37]),

$$\tilde{\mu}_v = \mu_v^{\circ} + f_{vv} n_v + f_{av} n_a + RT \ln \frac{n_v}{1 - n_v} + 2F \phi - \beta_v \nabla^2 n_v \quad (2a)$$

$$\tilde{\mu}_a = \mu_a^{\circ} + f_{aa} n_a + f_{av} n_v + RT \ln \frac{n_a}{1 - n_a} - F \phi - \beta_a \nabla^2 n_a, \quad (2b)$$

where  $f_{vv}$  and  $f_{aa}$  are defect self-interaction energies,  $f_{av}$  is the dopant–vacancy interaction energy, and  $\beta_v$  and  $\beta_a$  are gradient energy coefficients. In addition to the standard chemical potential, configurational and electrostatic terms of eqn (1), each electrochemical potential includes an excess chemical potential,<sup>38</sup> which can be divided into local ( $f$ ) and non-local ( $\beta$ ) terms; considered together, these terms comprise an effective activity coefficient. The sole assumptions, it is emphasised, that are made in deriving eqn (2) are that the local defect interactions can be represented by quadratic terms appearing in the free energy functional; that the free energy can be expanded in gradients of the concentration according to Cahn–Hilliard theory; and that crystal anisotropy can be neglected. The condition for equilibrium is, as before, that the electrochemical potentials of all mobile defects are constant throughout the system; the electrostatic potential follows Poisson’s equation.

Of critical importance (as shown below) are the gradient energy terms. They arise from symmetry breaking: spatially fluctuating defect concentrations prevent the formation of low-energy ordered configurations that extend in all directions. Gradient energy coefficients are thus strictly positive—they have been derived rigorously from first principles for the case of an Ising model.<sup>36</sup> In analogy to the electric field, this non-local chemical interaction is a force associated with the gradi-

ent of a scalar field: that of the chemical concentration. This is reflected in the elliptic form of the differential equations that arise upon equating the electrochemical potentials of eqn (2) with the electrochemical potential of the bulk: just as local charge density imparts curvature to the electrostatic potential according to Poisson's equation, a deviation of the local electrochemical potential from that of the bulk imparts curvature to the concentration field.

For simplicity we reduce the problem to one dimension,  $x \in [0, L]$ , which is appropriate for a sufficiently large grain size  $2L$ . The boundary conditions in the oxide bulk are fixed by the bulk dopant concentration, electroneutrality and the specification of a reference for the electrostatic potential. Because the theory does not consider the GB core to exist as a separate phase, there is no charge separation outside of the interval  $[0, L]$ , and the derivative of the electrostatic potential is therefore zero at the interface. The boundary conditions for vacancies and for dopants arise naturally from the variational analysis of the corresponding free energy functional:<sup>37</sup>

$$N\beta_{\text{def}} \left. \frac{dn_{\text{def}}}{dx} \right|_{x=0} = N^{\text{GB}} f_{\text{def}}^{\text{GB}}, \quad (3)$$

where  $N$  is the volumetric density of sites in the bulk,  $N^{\text{GB}}$  is the area-specific site density at the interface, and  $f_{\text{def}}^{\text{GB}}$  is the segregation energy and is given, as in the dilute case, by the difference in the standard chemical potential of def at the grain boundary and in the bulk.

Formulated in this manner, the model is a second-order, nonlinear boundary value problem (retaining the elliptic character of the Poisson–Boltzmann model) that can be solved with standard techniques. The results shown below were generated with a custom-built, adaptive finite-elements solution implemented in MATLAB (a version is available for download in the Supplementary Information†). Parameters used in the simulation appear in Table 1.

param.	value	comment
$f_{\text{vv}}$	0.9 eV	Ref. 11
$f_{\text{aa}}$	0.1 eV	Ref. 11
$f_{\text{av}}$	-0.07 eV	conductivity peak
$f_{\text{v}}^{\text{GB}}$	-2.0 eV	Ref. 23
$f_{\text{a}}^{\text{GB}}$	0 eV	
$N_{\text{v}}^{\text{GB}}$	$2.6 \times 10^{-5} \text{ mol m}^{-2}$	$2 \times$ ceria (111) termination
$\beta_{\text{v}}$	$0.125 \text{ eV nm}^2$	conductivity decrease
$\beta_{\text{a}}$	$2.5 \text{ eV nm}^2$	
$\epsilon_{\text{r}}$	35	
$N$	$2.49 \times 10^{28} \text{ m}^{-3}$	

**Table 1** Baseline parameter values

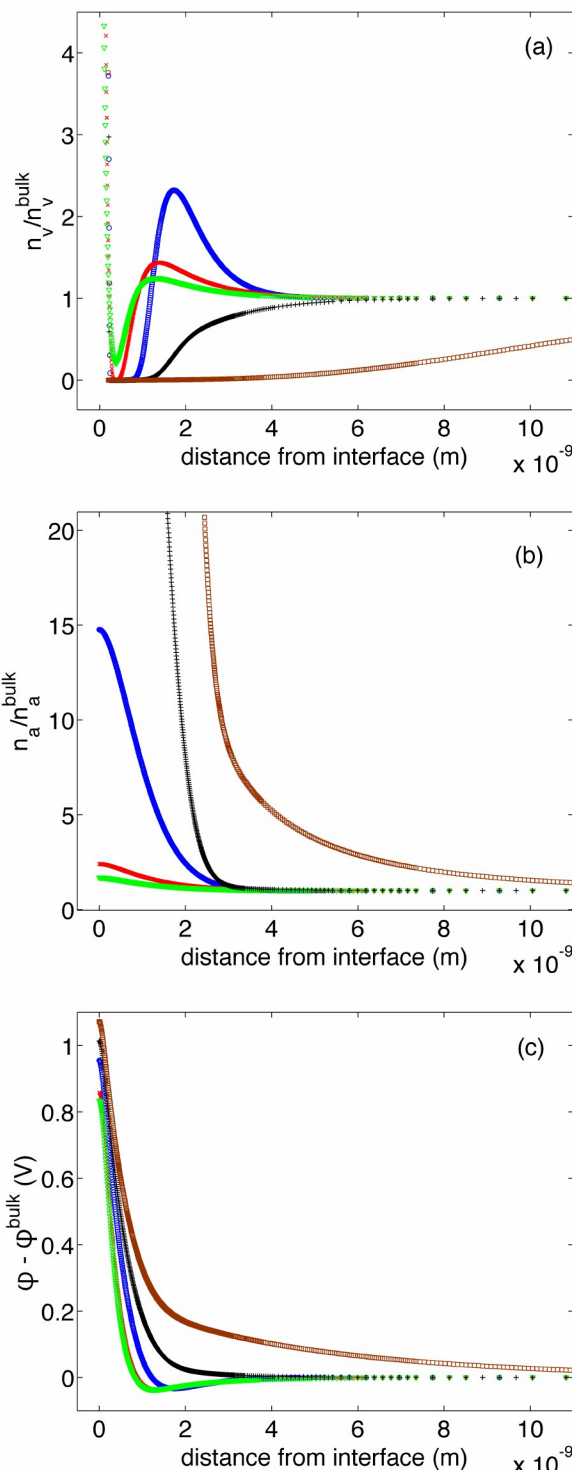


**Fig. 1** (a) Normalised vacancy concentration, (b) normalised dopant concentration and (c) electrostatic potential as a function of distance from the GB interface at 440 °C for bulk dopant concentrations of 0.01% ( $\square$ ), 0.1% (+), 1% ( $\circ$ ), 10% ( $\times$ ) and 20% ( $\nabla$ ). Parameters used in the simulation appear in Table 1

Fig. 1 shows defect-concentration and electrostatic-potential profiles calculated with the Poisson–Cahn theory for increasing bulk dopant concentrations. Starting with the vacancy-concentration profiles of Fig. 1(a), one sees, near the interface, steep increases in the vacancy concentration, which reflect the segregation of oxygen vacancies to the interface. This segregation zone has a finite thickness at all dopant concentrations, although it sharpens as concentrations decrease and defect interactions become correspondingly less important. Considering now the concentration profiles of vacancies and dopants together [Fig. 1(a) and (b)], one recognises the familiar dilute behaviour at 0.01% and 0.1% Gd: vacancy depletion is accompanied by dopant accumulation, and a strong increase in  $n_a^{\text{bulk}}$  leads to a strong decrease in the extent of the space-charge zone. This behaviour is in quantitative agreement with the standard Gouy–Chapman description.<sup>28,29,39</sup> At 1%, however, this standard description breaks down: the near-interface vacancy profile displays both depletion *and* enrichment; and it extends over 4 nm into the bulk, even as the Debye length drops to 0.3 nm. As  $n_a^{\text{bulk}}$  increases further, the depletion zone continues to shrink in severity and extent. By 20% dopant concentration (the highest value examined), the depletion of vacancies never falls below 20% of its bulk value, even though the space-charge potential is over 0.8 V.

Concentrations of vacancies and dopant cations at the interface are plotted in Figure 2 as a function of bulk dopant concentration (as the values are not apparent in Fig. 1). One finds that the composition of the interface is somewhat insensitive to changes in the bulk dopant concentration:  $n_v^{\text{GB}}$  increases by a factor of 0.3 and  $n_a^{\text{GB}}$  by a factor of 4, as  $n_a^{\text{bulk}}$  increases by a factor of  $10^3$ .

Good agreement is seen for the concentrated case between the Poisson–Cahn approach and atomistic simulations:<sup>26,33</sup> in both cases, changes in defect concentration—co-accumulation of dopants and vacancies, followed by a vacancy depletion region—occur over a length scale of several nm. Such behaviour can only arise in a continuum formulation from the chemical gradient energy, as this is the source of the long-range chemical interaction responsible for broadening the sharp accumulation profile of vacancies at the GB into the bulk phase. We emphasise this point by examining in Fig. 3 the effect of the gradient energy coefficient on near-interface oxygen-vacancy profiles for a relatively dilute composition (0.1% bulk dopant concentration) at 440 °C. At the lowest gradient energy, the enrichment region is very thin, and the corresponding vacancy depletion zone is approximately 1.5 nm wide. As the gradient energy coefficient increases, the enrichment region broadens into the bulk and the depletion zone shrinks in both size and severity, until at a value of  $\beta_v = 25.0$  eV nm<sup>2</sup> the minimum near-surface vacancy concentration is 30% of the bulk concentration. Not shown are the corresponding dopant concentration profiles, which also

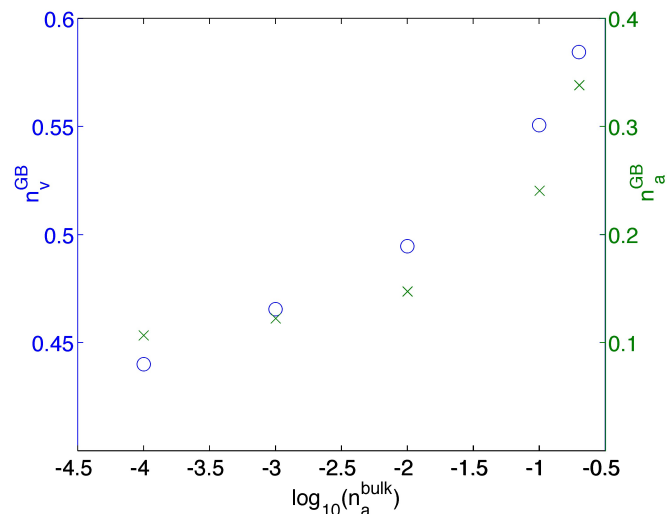


**Fig. 2** Oxygen-vacancy (○, left axis) and dopant-cation (×, right axis) site fractions at the interface for 440 °C according to the Poisson–Cahn simulations, using parameters appearing in Table 1

broaden as the vacancy gradient energy ( $\beta_v$ ) increases due to the vacancy–dopant attraction ( $f_{av}$ ). Parametric tests of the model reveal cases (especially those with higher gradient energy coefficients for oxygen vacancies) in which the depletion zone disappears altogether at high bulk dopant concentrations, with a co-enriched zone of dopant and vacancies in the near-interface region.

A critical test for any model of the near-interface defect structure is its ability to reproduce the experimentally observed changes in ionic conductivity with dopant concentration in polycrystalline materials. Figure 4 shows the ionic conductivity of the CeO<sub>2</sub>–Gd<sub>2</sub>O<sub>3</sub> system at 440 °C (separated into bulk and total contributions) predicted by combining the results of the Poisson–Cahn framework—with the parameter values listed in Table 1—together with a model for oxygen-ion conductivity in doped fluorite electrolytes given by Nakayama and Martin.<sup>7</sup> This model takes into account the effect of dopant–vacancy interactions on the mobility and the effect of dopants on the activation barriers for ion migration: as the local chemical environment (dopant and vacancy concentrations) varies with position within the space-charge layer, so will the local mobility of oxygen vacancies. Only nearest-neighbour and next-nearest-neighbour interactions are considered, and vacancy–vacancy interactions are not considered at all.\* Nevertheless, the combination of Poisson–Cahn theory and the Nakayama–Martin model reproduces qualitatively the behaviour over the entire concentration range of CeO<sub>2</sub>–Gd<sub>2</sub>O<sub>3</sub>

\* Grain size was controlled through varying the size of the simulation domain; the grain size used to produce these results was 20 μm. Only conductivity perpendicular to the grain boundaries was considered.

(cf. experimental data from Tschöpe *et al.*<sup>23</sup> shown in the inset). The lack of consideration of vacancy–vacancy repulsion in the model for vacancy mobility may explain the remaining gap in the bulk conductivity and peak total conductivity, as suggested by Nakayama and Martin.<sup>7</sup> However, the salient finding is that the Poisson–Cahn model is capable of reproducing the qualitative behavior of the total conductivity seen in experiment from the dilute case through to the concentrated case. Tschöpe *et al.*,<sup>23</sup> in contrast, were only able to demonstrate agreement with their experimental results up to a few percent doping concentration, just short of the conductivity maximum seen in Fig. 4. This is in part because significant defect interactions are likely to be present for bulk defect concentrations on the order of 1%. It is also in part because the vacancy mobility is assumed to be constant within the space-charge zone: Consideration of Figs. 1 and 4 indicates that the GB resistance at low  $n_a^{\text{bulk}}$  is due to a concentration effect (strong depletion of charge carriers), whereas at high  $n_a^{\text{bulk}}$ , as the degree of depletion lessens, it is the diminished mobility that becomes increasingly important.

We note that three of the interaction parameters appearing in Table 1 were calculated by means of density-functional-theory calculations (citations appear in the table), while two were adjusted in order to bring the results into closer accord with experiment. The dopant–vacancy interaction energy was adjusted to produce the peak conductivity at a dopant concentration similar to what is seen in the experiment; still, at

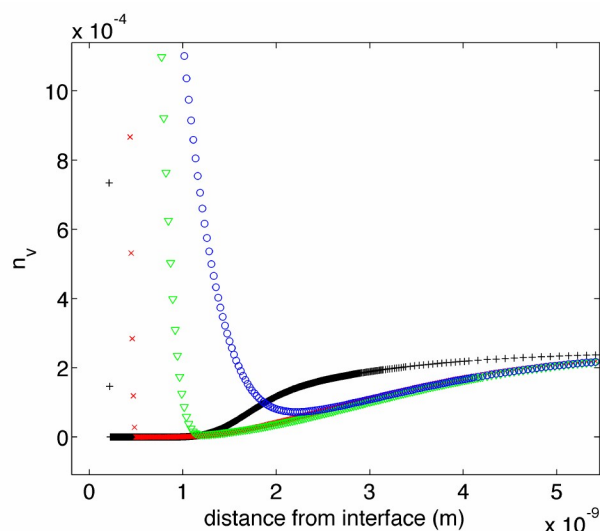


**Fig. 3** Oxygen-vacancy profiles as a function of distance from the interface at 440 °C for a (dilute) bulk dopant concentration of 0.1%. The parameters used in the simulation are those in Table 1 except for the vacancy gradient energy coefficient ( $\beta_v$ ), which is varied:  $\beta_v = 0.125 \text{ eV-nm}^2$  (+),  $\beta_v = 1.25 \text{ eV-nm}^2$  ( $\times$ ),  $\beta_v = 12.5 \text{ eV-nm}^2$  ( $\nabla$ ),  $\beta_v = 25.0 \text{ eV-nm}^2$  ( $\circ$ )

$f_{\text{av}} = -0.07 \text{ eV}$ , the value is reasonably close to the DFT-calculated value of  $-0.3 \text{ eV}$ .<sup>11</sup> The gradient energy coefficient for vacancies was adjusted to replicate the precipitous decrease in total conductivity with decreasing dopant concentration seen in experiment. (The coefficient for Gd was fixed at a physically reasonable, but otherwise arbitrary value.) The number of oxygen sites at the interface per unit area was chosen as two times value obtained by considering a smooth (111) termination of a  $\text{CeO}_2$  lattice, reflecting the atomistically rough nature of the interface. This value is sufficiently large that the number of interface sites does not limit the number of vacancies transferred from the bulk to the interface.<sup>29</sup> It is also noted that these parameters are not unique but they are all physically reasonable. More importantly, when used as input into the framework of Poisson–Cahn, they reproduce various aspects of observed behaviour from dilute to concentrated systems in a theoretically consistent manner.

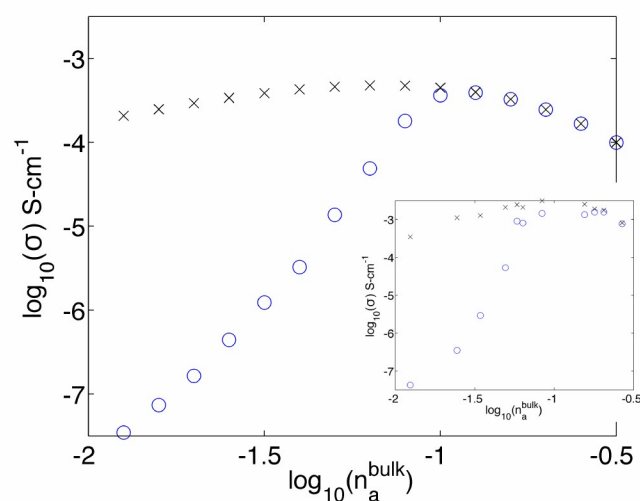


**Fig. 4** Bulk ( $\times$ ) and total ( $\circ$ ) conductivity for gadolinia-doped ceria at 440 °C, generated from the Poisson–Cahn model for equilibrium defect concentrations and the Nakayama–Martin model for defect mobility in concentrated fluorite electrolytes. Parameters used in the model are those appearing in Table 1. Inset: experimental data for gadolinia-doped ceria from Tschöpe *et al.*<sup>23</sup>

## Conclusions

The Poisson–Cahn theory extends the framework of the continuum space-charge treatment near surfaces and interfaces from the dilute to the concentrated case. It conforms to the dilute Poisson–Boltzmann (Gouy–Chapman) case in the limit of small dopant concentrations, showing a vacancy depletion zone whose extent broadens as bulk dopant concentrations decrease. It also conforms to the results of atomistic simulations

in the concentrated case, which show variously co-enrichment of vacancies and dopant or shallow depletion followed by enrichment of vacancies. The formalism reproduced qualitatively the experimental conductivity behaviour of polycrystalline gadolinia-doped ceria as a function of dopant concentration. The origin of GB resistance remains the appearance of space-charge zones whose formation is driven by the segregation of oxygen vacancies to the interface. The importance of considering changes in both the concentration and the mobility of charge carriers in space-charge regions is emphasised.

## References

- 1 T. H. Etsell and S. N. Flengas, *Chem. Rev.*, 1970, **70**, 339–376.
- 2 J. C. Boivin and G. Mairesse, *Chem. Mater.*, 1998, **10**, 2870–2888.
- 3 B. C. H. Steele and A. Heinzl, *Nature*, 2001, **414**, 345–352.
- 4 J. B. Goodenough, *Ann. Rev. Mater. Res.*, 2003, **33**, 91–128.
- 5 M. Meyer, N. Nicoloso and V. Jaenisch, *Phys. Rev. B*, 1997, **56**, 5961–5966.
- 6 R. Pornprasertsuk, P. Ramanarayanan, C. B. Musgrave and F. B. Prinz, *J. Appl. Phys.*, 2005, **98**, 103513.
- 7 M. Nakayama and M. Martin, *Phys. Chem. Chem. Phys.*, 2009, **11**, 3241–3249.
- 8 B. Grope, T. Zacherle, M. Nakayama and M. Martin, *Solid State Ionics*, 2012, **225**, 476–483.
- 9 P. P. Dholabhai, S. Anwar, J. B. Adams, P. A. Crozier and R. Sharma, *Modelling Simul. Mater. Sci. Eng.*, 2012, **20**, 015004.
- 10 H. Wang, A. Chroneos and U. Schwingenschlgl, *J. Chem. Phys.*, 2013, **138**, 224705.
- 11 S. Grieshammer, B. O. H. Grope, J. Koettgen and M. Martin, *Phys. Chem. Chem. Phys.*, 2014, **16**, 9974–9986.
- 12 N. Beekmans and L. Heyne, *Electrochim. Acta*, 1976, **21**, 303–310.
- 13 M. Verkerk, B. Middelhuis and A. Burggraaf, *Solid State Ionics*, 1982, **6**, 159–170.
- 14 A. I. Ioffe, M. V. Inozemtsev, A. S. Lipilin, M. V. Perfilev and S. V. Karpachov, *phys. status solidi (a)*, 1975, **30**, 87–95.
- 15 D. Y. Wang and A. Nowick, *J. Solid State Chem.*, 1980, **35**, 325–333.
- 16 M. Kleitz, L. Dessemond and M. Steil, *Solid State Ionics*, 1995, **75**, 107–115.
- 17 M. Gdickemeier, B. Michel, A. Orliukas, P. Bohac, K. Sasaki, L. Gauckler, H. Heinrich, P. Schwander, G. Kostorz, H. Hofmann and O. Frei, *J. Mater. Res.*, 1994, **9**, 1228–1240.
- 18 S. Badwal and J. Drennan, *Solid State Ionics*, 1990, **40-41, Part 2**, 869–873.
- 19 R. Gerhardt and A. S. Nowick, *J. Am. Ceram. Soc.*, 1986, **69**, 641–646.
- 20 G. Christie and F. van Berkel, *Solid State Ionics*, 1996, **83**, 17–27.
- 21 J.-S. Lee and D.-Y. Kim, *J. Mater. Res.*, 2001, **16**, 2739–2751.
- 22 X. Guo, W. Sigle and J. Maier, *J. Am. Ceram. Soc.*, 2003, **86**, 77–87.
- 23 A. Tschöpe, S. Kilassonia and R. Birringer, *Solid State Ionics*, 2004, **173**, 57–61.
- 24 H. J. Avila-Paredes, K. Choi, C.-T. Chen and S. Kim, *J. Mater. Chem.*, 2009, **19**, 4837–4842.
- 25 D. Bingham, P. W. Tasker and A. N. Cormack, *Phil. Mag. A*, 1989, **60**, 1–14.
- 26 H. B. Lee, F. B. Prinz and W. Cai, *Acta Mater.*, 2013, **61**, 3872–3887.
- 27 D. R. Franceschetti, *Solid State Ionics*, 1981, **2**, 39–42.
- 28 J. Maier, *Prog. Solid State Chem.*, 1995, **23**, 171–263.
- 29 R. A. De Souza, *Phys. Chem. Chem. Phys.*, 2009, **11**, 9939–9969.
- 30 J. Jamnik, J. Maier and S. Pejovnik, *Solid State Ionics*, 1995, **75**, 51–58.
- 31 S. K. Kim, S. Khodorov, I. Lubomirsky and S. Kim, *Phys. Chem. Chem. Phys.*, 2014, **16**, 14961–14968.
- 32 N. Shibata, Y. Ikuhara, F. Oba, T. Yamamoto and T. Sakuma, *Phil. Mag. Lett.*, 2002, **82**, 393–400.
- 33 H. B. Lee, F. B. Prinz and W. Cai, *Acta Mater.*, 2010, **58**, 2197–2206.
- 34 J. W. Cahn and J. E. Hilliard, *J. Chem. Phys.*, 1958, **28**, 258–267.
- 35 J. W. Cahn, *J. Chem. Phys.*, 1977, **66**, 3667–3672.
- 36 S. Puri and K. Binder, *Phys. Rev. A*, 1992, **46**, R4487–R4489.
- 37 D. S. Mebane, *Comput. Mater. Sci.*, 2015, **103**, 231–236.
- 38 J. Maier, *Nature Mater.*, 2005, **4**, 805–815.
- 39 N. Uvarov, *Solid State Ionics*, 2008, **179**, 783–787.